

Composite fermionization of one-dimensional Bose-Bose mixtures

Sascha Zöllner,^{1,*} Hans-Dieter Meyer,¹ and Peter Schmelcher^{1,2,†}

¹*Theoretische Chemie, Universität Heidelberg, INF 229, 69120 Heidelberg, Germany*

²*Physikalisches Institut, Universität Heidelberg, Philosophenweg 12, 69120 Heidelberg, Germany*

(Received 5 May 2008; published 22 July 2008)

We study the ground states of one-dimensional Bose-Bose mixtures under harmonic confinement. As we vary the interspecies coupling strength up to the limit of infinite repulsion, we observe a generalized, composite-fermionization crossover. The initially coexisting phases demix as a whole for weak intraspecies interactions, whereas the atoms localize individually for strong intraspecies repulsion. By symmetry, the two components end up with strongly overlapping profiles, albeit sensitive to symmetry-breaking perturbations. Different pathways emerge if the two components have different atom numbers, different intraspecies interactions, or different masses and/or trap frequencies.

DOI: 10.1103/PhysRevA.78.013629

PACS number(s): 67.85.-d, 67.60.Bc, 03.75.Mn

I. INTRODUCTION

The availability of cold atoms has made it possible to realize many fundamental quantum systems. Building on the seminal realization of Bose-Einstein condensation [1,2], mixtures composed of, say, two different atomic species have come into the research focus. Aside from Bose-Fermi [3,4] or Fermi-Fermi mixtures [5], whose potential for studying phenomena as diverse as impurity effects or superconductivity has been recognized more recently, two-component bosonic mixtures have received much experimental [6–10] and theoretical attention (see [11–18] and references therein). The interplay between intra- and interspecies forces gives rise to many effects not accessible with single-component Bose gases, including phase separation and modified superfluid-insulator transitions [14,15], quantum emulsions [16], and spin-charge separation [18].

Most studies so far have focused on the regime of relatively weak interactions, where the physics can be described well in terms of mean-field or—in lattice geometries—simple lowest-band models. However, interatomic forces can be experimentally tuned to a large extent via Feshbach resonances [19]. In particular, in quasi-one-dimensional systems, which emerge under strong transverse confinement, it is possible to exploit confinement-induced resonances [20] to explore the regime of strong correlations [21,22]. For infinitely repulsive bosons, this is known as the fermionization limit, in allusion to the fact that the system can be mapped exactly to an ideal Fermi gas [23]. Here the exclusion principle in a sense emulates the effect of *hard-core* interactions, to the extent that the bosons share local aspects with their fermionic counterparts, whereas nonlocal properties such as their coherence and momentum distribution are very different. The basic crossover from the weakly interacting trapped Bose gas to the fermionization limit had been predicted from a thermodynamic-limit perspective [24,25]. The pathway for finite systems and specifically its trap dependence has been identified via a multiorbital mean-field approach [26]. By

contrast, it is only recently that its *microscopic* mechanism has been investigated within an *ab initio* framework [27–30].

In this work, we tackle the obvious question of how the fermionization crossover for the one-component Bose gas extends to a trapped *two-component* mixture. By way of analogy, tuning the *intercomponent* coupling strength to the infinitely repulsive regime (for fixed intraspecies interactions) may be regarded as *composite fermionization*. Here, a recent study has extended the standard fermionization map to mixtures of two identical particle species with both intra- and interspecies hard-core interactions [31]. Apart from this special borderline case, little is known except for a classification of the low-energy modes in the harmonic-fluid approximation [11]. Here we study the crossover from weak to strongly repulsive couplings between two components under harmonic confinement. We will show that this composite fermionization can lead to demixing, and lay out how it depends on the intraspecies interactions, on the densities of the two components, as well as on the masses and trapping parameters of each species.

Our paper is organized as follows. Section II introduces the model and briefly reviews the fermionization map and its extension to mixtures. In Sec. III, we give a concise presentation of the computational method. Section IV first explores the completely symmetric setup, where both components have equal atom numbers, interaction constants, masses, and see the same harmonic trap. The subsequent Sec. V in turn shows what different phase-separation scenarios emerge if these constraints are relaxed one by one.

II. THEORETICAL BACKGROUND

A. Model

We consider a mixture of two distinguishable bosonic species, which we shall label *A* and *B*. These may correspond to atoms with unequal nucleon numbers—be it different isotopes or altogether different species—or possibly different hyperfine states of one and the same species. Furthermore, we assume these to be confined to quasi-one dimension (1D), such that the transverse degrees of freedom may be integrated out. The effective low-energy Hamiltonian for an ar-

*sascha.zoellner@pci.uni-heidelberg.de

†peter.schmelcher@pci.uni-heidelberg.de

bitrary mixture of $N=N_A+N_B$ atoms then reads

$$H = \sum_{\sigma=A,B} H_{\sigma} + H_{AB},$$

where the single-species Hamiltonian H_{σ} and the interspecies coupling H_{AB} read

$$H_{\sigma} = \sum_{i=1}^{N_{\sigma}} \left(\frac{p_{\sigma,i}^2}{2M_{\sigma}} + U_{\sigma}(x_{\sigma,i}) \right) + \sum_{i<j} g_{\sigma} \delta(x_{\sigma,i} - x_{\sigma,j}),$$

$$H_{AB} = \sum_{a=1}^{N_A} \sum_{b=1}^{N_B} g_{AB} \delta(x_{A,a} - x_{B,b}).$$

Here we consider harmonic trapping potentials $U_{\sigma}(x) = \frac{1}{2} M_{\sigma} \omega_{\sigma}^2 x^2$. By rescaling to harmonic-oscillator units $a_A \equiv \sqrt{\hbar / M_A \omega_A}$, one can eliminate $M_A = \omega_A = 1$ by exploiting the scaling

$$H_A(M_A, \omega_A, g_A; X_A) = \hbar \omega_A H_A(1, 1, g'_A; X'_A),$$

with $X'_A \equiv (x'_{A,1}, \dots, x'_{A,N_A}) \equiv X_A / a_A$ and $g'_A \equiv g_A \sqrt{M_A / \hbar^3} \omega_A$.

For numerical reasons, we regularize the δ -function interaction by a normalized Gaussian of width much smaller than the interparticle distance; see Ref. [28] for details.

B. Fermionization

The (single-component) 1D Bose gas has the peculiar property that it is isomorphic to a system of identical fermions. In particular, the *standard* Bose-Fermi map relates the many-body wave function of hard-core bosons (obeying the boundary condition $\Psi|_{x_i=x_j} = 0$, $i < j$, which corresponds to taking the 1D interaction strength $g \rightarrow \infty$) to that of noninteracting fermions Ψ_- :

$$\Psi = A \Psi_-, \quad A(X) := \prod_{i<j} \text{sgn}(x_i - x_j).$$

Specifically, the ground state is given simply by the absolute value of the noninteracting fermionic ground state, $\Psi_0 = |\Psi_{-,0}|$. This makes it tempting to think of Pauli's exclusion principle as emulating the effect of the repulsive interactions (or vice versa), which is why the limit $g \rightarrow \infty$ is commonly referred to as fermionization. Note that, since $A^2 = 1$, all local quantities will coincide with those computed from the fermion state. Specifically, this is the case for the density $\rho_N = |\Psi|^2$ and any derived quantities, such as the reduced (one- or two-body) densities. However, nonlocal quantities such as the momentum distribution may differ dramatically from the fermionic ones.

The standard Bose-Fermi map above has recently been extended to mixtures of two identical species $A=B$ (i.e., equal masses and potentials) with hard-core intra- and interspecies interactions, $g_{\sigma} = g_{AB} \rightarrow \infty$. Its wave function Ψ is transformed to that of a system of $N = \sum_{\sigma} N_{\sigma}$ identical fermions [31]. For the special case of A and B being bosonic, this *generalized* Bose-Fermi map $\Psi = A \Psi_-$ reads

$$A(X_A, X_B) = A_A(X_A) A_B(X_B) A_{AB}(X_A, X_B), \quad (1)$$

where $A_{\sigma}(X_{\sigma}) \equiv \prod_{1 \leq i < j \leq N_{\sigma}} \text{sgn}(x_{\sigma,i} - x_{\sigma,j})$ is the standard map restricted to subsystem σ , and $A_{AB}(X_A, X_B) \equiv \prod_{a=1}^{N_A} \prod_{b=1}^{N_B} \text{sgn}(x_{A,a} - x_{B,b})$ serves to impose hard-core boundary conditions on interspecies collision points. In the case of harmonic trapping, where the single-particle orbitals are known analytically, the solution may even be written down explicitly [31],

$$\Psi(X \equiv (X_A, X_B)) \propto e^{-|X|^2/2} \prod_{1 \leq i < j \leq N} |x_i - x_j|. \quad (2)$$

III. COMPUTATIONAL METHOD

Our approach relies on the numerically exact multiconfiguration time-dependent Hartree method [32,33], a quantum-dynamics tool which has been applied successfully to systems of a few identical bosons (see [28,29,34–36]). Its principal idea is to solve the time-dependent Schrödinger equation $i\dot{\Psi}(t) = H\Psi(t)$ as an initial-value problem by expanding the solution in terms of direct (or Hartree) products $\Phi_J \equiv \varphi_{j_1}^{(1)} \otimes \dots \otimes \varphi_{j_N}^{(N)}$:

$$\Psi(t) = \sum_J A_J(t) \Phi_J(t). \quad (3)$$

The (unknown) single-particle functions $\varphi_j^{(\kappa)}$ ($j=1, \dots, n_{\kappa}$) are in turn represented in a fixed primitive basis implemented on a grid. In our case, where particles of each species are indistinguishable, the single-particle functions within each subset $\kappa \in \{1, \dots, N_A\}$ and $\{N_A+1, \dots, N\}$ are of course identical (i.e., we have $\{\varphi_{j_{\sigma}}^{(\sigma)}\}$, with $j_{\sigma} \leq n_{\sigma}$). This, along with the correct symmetrization of the expansion coefficients A_J , ensures permutation symmetry within each subset A, B .

Note that in the above expansion not only the coefficients A_J but also the single-particle functions φ_j are time dependent. Using the Dirac-Frenkel variational principle, one can derive equations of motion for both A_J and φ_j [33]. Integrating this differential-equation system allows us to obtain the time evolution of the system via (3). This has the advantage that the basis $\{\Phi_J(t)\}$ is variationally optimal at each time t . Thus it can be kept relatively small, rendering the procedure very efficient.

Although designed for time-dependent simulations, it is also possible to apply this approach to stationary states. This is done via the so-called *relaxation method* [37]. The key idea is to propagate some wave function $\Psi(0)$ by the non-unitary $e^{-H\tau}$ (propagation in imaginary time). As $\tau \rightarrow \infty$, this exponentially damps out any contribution but that stemming from the true ground state like $e^{-(E_m - E_0)\tau}$. In practice, one relies on a more sophisticated scheme termed *improved relaxation* [38], which is much more robust especially for excitations. Here $\langle \Psi | H | \Psi \rangle$ is minimized with respect to both the coefficients A_J and the orbitals φ_j . The effective eigenvalue problems thus obtained are then solved iteratively by first solving for A_J with fixed orbitals and then “optimizing” φ_j by propagating them in imaginary time over a short period. That cycle will then be repeated.

IV. COMPOSITE-FERMIONIZATION TRANSITION

In contrast to the case of a single bosonic species, binary mixtures offer a plethora of different parameters, making the physics richer and less straightforward: In principle, we may have different atom numbers $N=N_A+N_B$, different masses $M_{\sigma=A,B}$, intra- and interspecies couplings g_σ (g_{AB}), and species-dependent traps $U_\sigma(x)$. In this section, in order to illustrate the basic mechanism of the crossover from weak to strongly repulsive interspecies interactions, $g_{AB} \in [0, \infty)$, we focus on the simplest, symmetric setup where

$$N_\sigma = \frac{N}{2}, \quad M_\sigma = 1, \quad g_\sigma = g, \quad U_\sigma(x) = \frac{1}{2}x^2 \quad (\sigma = A, B).$$

In this case, H has an exact permutation symmetry between species A and B . This idealized situation may correspond to two internal states of the same species or, ignoring slight mass deviations, two different isotopes, where g_{AB} is tuned via the interspecies scattering length. Actually, in the special case where $g_\sigma = g_{AB} = g$, this system maps to a one-component Bose gas with $N = \sum_\sigma N_\sigma$ atoms [28–30] (for any number of components and any N_σ for that matter)—up to permutational degeneracies, which are not very severe for the ground state.

Here, by contrast, we are interested in the following question: What happens to the mixture— g_σ being fixed—when g_{AB} is varied up to the hard-core limit? [This we refer to as *composite fermionization* of the subsystems A and B , despite the general lack of a Bose-Fermi mapping as in Eq. (1).] To get an impression of that crossover, let us start with the case of two almost ideal Bose gases, $g_\sigma = 0.4$, each consisting of $N_\sigma = 2$ atoms (similar results hold for larger atom numbers). Figure 1 displays the evolution of the density profile $\rho(x) \equiv \rho_\sigma(x)$, measuring the probability distribution for finding one σ atom at position x . Obviously, for $g_{AB} \rightarrow 0$, the total state $\Psi = \Psi_A \otimes \Psi_B$ simply consists of two uncorrelated “condensates” ($\Psi_\sigma = \phi_0^{\otimes N_\sigma}$ for $g=0$), slightly smeared out due to repulsion. Increasing g_{AB} leads to an ever deeper dip in the profiles. This should be contrasted with the case of two *single* fermionized bosons, $N_\sigma = 1$ [39]. The dip in Fig. 1 is much more pronounced, which is indicative of phase separation, if symmetry screened: $\rho_A = \rho_B$ are completely identical by symmetry. However, this only corresponds to an ensemble average—in a single measurement, we will always find all N_A atoms on one side of the trap and N_B atoms on the other. This claim is underscored by Fig. 1(bottom), which reveals the evolution of the two-body densities $\rho_{\sigma\sigma}(x_1, x_2) = \langle x_1, x_2 | \rho_\sigma^{(2)} | x_1, x_2 \rangle$ and $\rho_{AB}(x_A, x_B)$, obtained as usual from the total density matrix $\rho^{(N)} = |\Psi\rangle\langle\Psi|$ by tracing out all but two degrees of freedom (either from the same species σ or from different ones $A \neq B$). If we measure, say, the first A -type boson at $x_{A,1} \approx 1$, then we are sure to find the second A boson also in that region $x_{A,2} \approx 1$ and not on the left, and vice versa. By contrast, the probability for subsequently finding a B particle at the same position is virtually zero, as dictated by the hard-core boundary condition $\Psi|_{x_{A,a}=x_{B,b}} = 0$ ($g_{AB} \rightarrow \infty$). This makes it tempting to think of this as an entangled state of the form

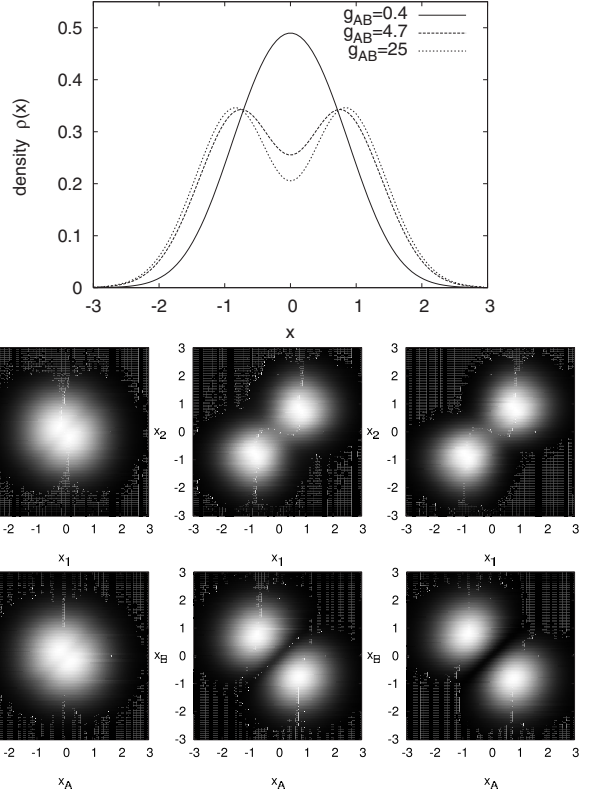


FIG. 1. Composite fermionization of a mixture with $N_{\sigma=A,B} = 2$ bosons with intracomponent interaction $g_\sigma = 0.4$. Top: density profiles $\rho(x)$; bottom: two-body correlation functions $\rho_{\sigma\sigma}(x_1, x_2)$ and $\rho_{AB}(x_A, x_B)$ for interspecies couplings $g_{AB} = 0.4, 4.7$, and 25 , from left to right. (All quantities in harmonic-oscillator units throughout; see text.)

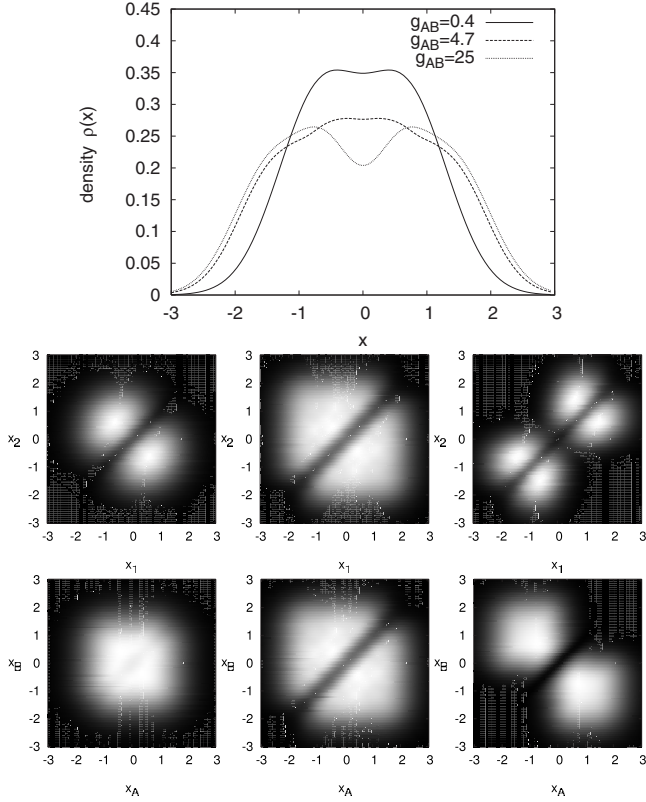
$$|N_A, 0\rangle \otimes |0, N_B\rangle + |0, N_A\rangle \otimes |N_B, 0\rangle,$$

where $|n_L, n_R\rangle \in \mathbb{H}_\sigma$ denotes a state with n_L (n_R) atoms localized on the left (right). It should be noted that, even for $g_\sigma = 0$, there is no simple mapping to fermions as in (1), since the hard-core condition is imposed only on interspecies collision points, and thus the information about which fragment the individual coordinates belong to needs to be retained. However, in our special case of a harmonic trap, it is tempting to modify the exact solution of the single-species fermionization limit [40],

$$\Psi_{g_{AB} \rightarrow \infty}(\mathbf{X}) \approx c e^{-|\mathbf{X}|^2/2} \prod_{a \leq N_A, b \leq N_B} |x_{A,a} - x_{B,b}|,$$

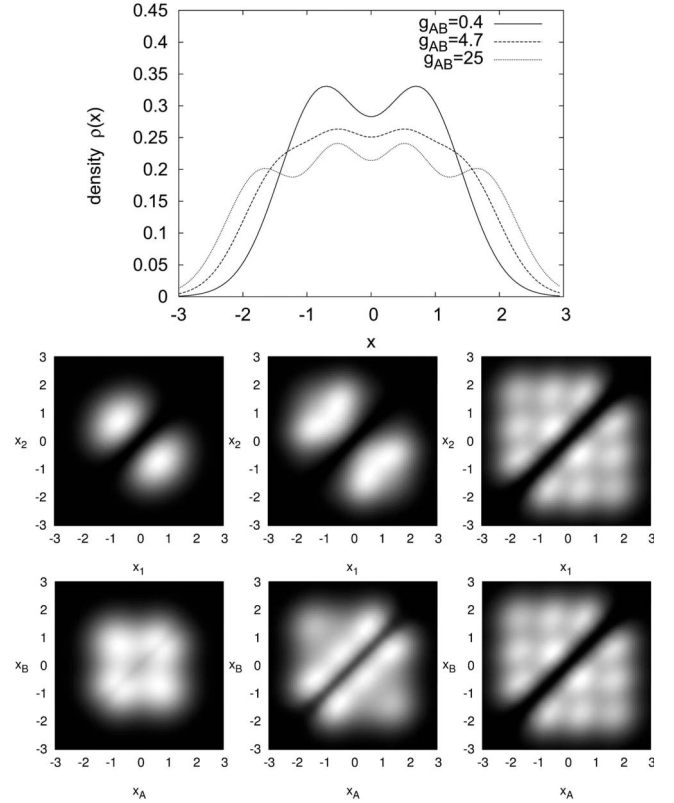
which obeys the correct boundary conditions at points of interspecies collisions. Even though in general it is not an exact eigenstate, it is expected to give an approximation. Trusting that logic, an analogous extension should hold for the homogeneous system [23].

A similar pathway is encountered for two more strongly interacting components, $g_\sigma = 4.7$ (see Fig. 2, top). At $g_{AB} = 0.4$, we have two more or less uncorrelated clouds, which are governed by the desire to reduce their *intraspecies* interaction energy. As $g_{AB} = 4.7$ reaches g_σ , there is a trade-off between avoiding the same species and avoiding the other


 FIG. 2. Same as Fig. 1, but with $g_A = g_B = 4.7$.

component. Letting $g_{AB} \rightarrow \infty$, the interparticle repulsion takes over, and a similar phase-separation tendency of A and B as before may be recognized in Fig. 2. In contrast to the “condensate” case, however, the separation of the two peaks is not pronounced as each hump is quite smeared out in itself due to the intraspecies repulsion. This is illuminated further by the two-body densities (Fig. 2): Here the pattern for $\rho_{\sigma\sigma}(x_1, x_2)$ at $g_{AB}=25$ is modulated by a correlation hole at $x_1=x_2$ due to intraspecies repulsion, as compared to the weakly interacting components (Fig. 1). This explains the two broadened peaks in $\rho_{\sigma}(x)$.

So far, we have seen that the components tend to separate when the interspecies repulsion overwhelms the intraspecies one. This naturally brings up the question of the fate of two initially fermionized components, as shown for $g_{\sigma}=25$ in Fig. 3. Notably, by the conventional Bose-Fermi map, this relates to a Fermi-Fermi mixture. Weak couplings $g_{AB}=0.4$ pass the two fermionized clouds largely unnoticed, which exhibit $N_{\sigma}=2$ characteristic humps in $\rho_{\sigma}(x)$ [28,30]. However, for larger values $g_{AB}=4.7$, the profiles slowly rearrange to a more complex structure, which culminates in a profile with $N=4$ wiggles at $g_{AB}=g_{\sigma}=25$. The density oscillations signify that *each* of the four atoms seeks an isolated spot, irrespective of its species. That interpretation is supported by the plots of the two-body densities $\rho_{\sigma\sigma}=\rho_{AB}$, which for $g_{AB}=25$ reveal the checkerboard pattern familiar from the single-boson crossover [28]. This should be contrasted with the intermediate regime where $g_{AB}=4.7 < g_{\sigma}$: Here two, say, A atoms are still localized on the left and on the right side as for $g_{AB}=0$. Upon measuring an A atom at, say, $x_A \approx 1.5$, the two B atoms will likely be found at either $x_B \approx 0.5$ or x_B


 FIG. 3. Same as Fig. 1, but with $g_A = g_B = 25$.

≈ -1.5 , in this way remaining isolated from each other but also avoiding the A atom.

Note that, in agreement with our earlier remarks, the case $g_{\sigma}=g_{AB}$ relates to a single-component Bose gas, which in turn maps to an ideal *Fermi* gas via (1) in the limit $g_{AB} \rightarrow \infty$. As in that case, for $N \gg 1$ these N peaks become ever tinier modulations on the envelope density, which for a harmonic trap can be computed as $\bar{\rho}(x) = \sqrt{2N-x^2}/N\pi$ [41].

At this stage, we should point out that this limit is highly degenerate: For one thing, there is a permutation degeneracy between A and B particles. Second, in the limit $g_{AB} \rightarrow \infty$, the ground-state wave function (which is non-negative) degenerates with the fermionic one by the Bose-Fermi map and, since no specific permutation symmetry is imposed when treating the two components as distinguishable, all solutions even with mixed A - B exchange statistics are permissible [31].

Symmetry-breaking instability

By permutation symmetry of H between A and B , the density profiles ρ_{σ} are identical, even in the limit $g_{AB} \gg g_{\sigma}$ and thus trivially cannot exhibit phase separation. However, if we deal with two different species, it is conceivable that these two experience slightly different trapping potentials, where the deviations are much weaker than the mean trapping and interparticle forces but serve only to break the symmetry. In particular, imagine that $U_{\sigma}(x) = \frac{1}{2}x^2 + d_{\sigma}x$, such that the trap centers are shifted by $d_A = -d_B \ll 1$; see Fig. 4. As expected, for weak couplings g_{AB} , the profiles are barely af-

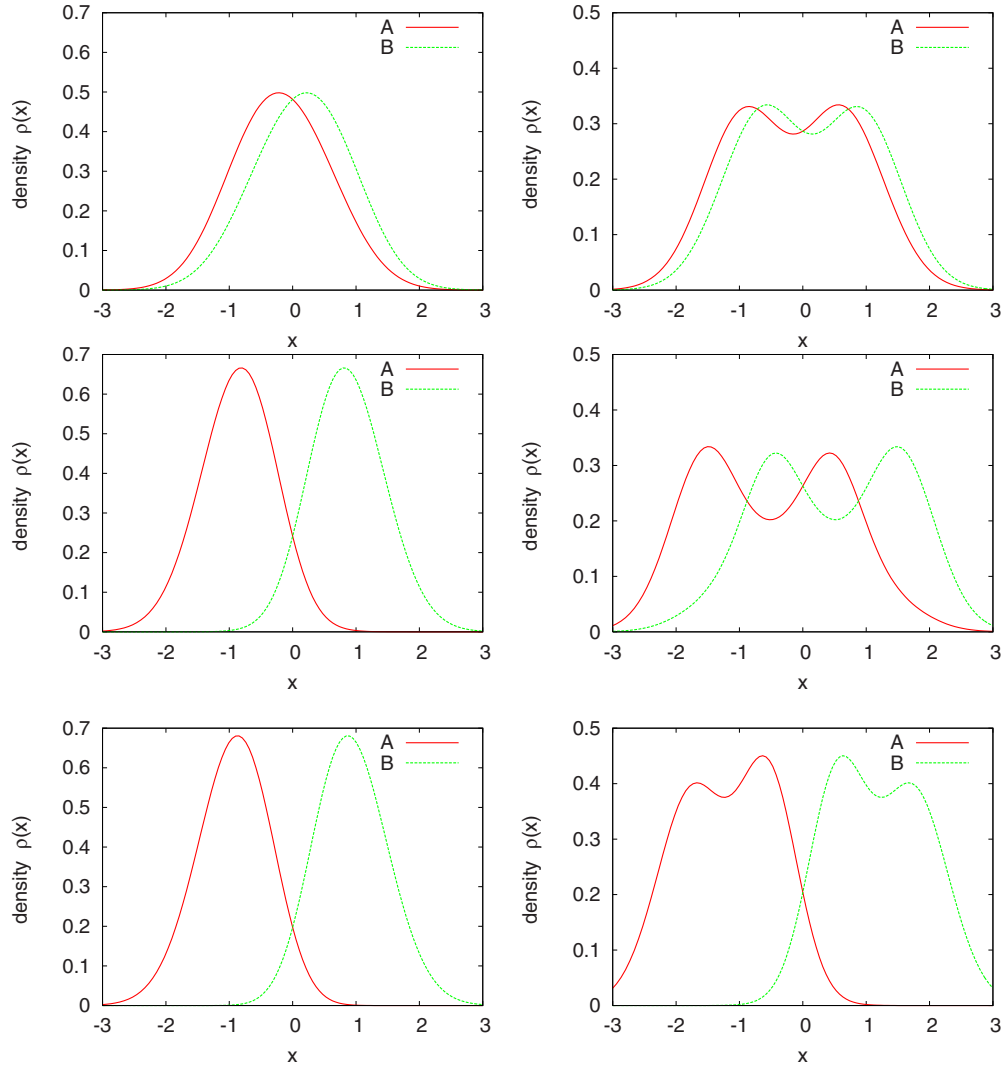


FIG. 4. (Color online) Instability under symmetry-breaking perturbation, $U_\sigma(x) = \frac{1}{2}x^2 + d_\sigma x$ ($d_A = -d_B = 0.1$). Left: Densities $\rho_\sigma(x)$ for $g_\sigma = 0.4$; right: $g_\sigma = 25$. Shown are the coupling strengths $g_{AB} = 0.4, 4.7, 25$ from top to bottom.

ected. However, toward stronger interspecies repulsion, this tiny perturbation is the last straw needed to make the two phases demix completely. Similar results hold also for different densities, $N_A \neq N_B$. This makes it even more inviting to think of the symmetric profiles in Figs. 1–3 as averages over the equivalent configurations with A (B) being on the left (right), and the other way around. The symmetry-broken profiles in Fig. 4 are reminiscent of those in Ref. [14], which demonstrated that demixing in *optical lattices* occurs on different length scales. Here we show that similar conclusions apply even in a single-well trap, solely due to interactions.

V. PHASE-SEPARATION SCENARIOS

So far, we have studied a completely symmetric setup, where only the interspecies interactions were permitted to differ. In this way, a symmetry-breaking perturbation was needed to reveal the hidden phase separation. Although not experimentally unrealistic, this scenario is somewhat artificial. We now want to relax the above symmetry constraints

step by step and discuss the wealth of different demixing pathways if the two components have different particle numbers (Sec. V A), different internal interaction strengths (Sec. V B), and have different masses and/or trap frequencies (Sec. V C).

A. Density-assisted demixing

There is an obvious question regarding our findings in the previous section: What happens in the case of unequal particle numbers, $N_A \neq N_B$? Figure 5 illustrates this on the example of two weakly interacting components, $g_\sigma = 0.4$ (left column), where $N_A = 3$ is larger than $N_B = 2$. As the Bose-Bose coupling gets stronger, $g_{AB} = 1.3$, one observes that the low-density phase B moves to the outer edge, thus “sandwiching” high-density A component in the middle. This well-known phenomenon traces back to the fact that the coupling energy $\langle H_{AB} \rangle = N_A N_B g_{AB} \int \rho_{AB}(x, x) dx$ scales with $N_A N_B$ compared to the individual energies $\langle H_\sigma \rangle \propto N_\sigma$. Thus for the smaller B component, it is less expensive to move to the higher-potential regions. Not unexpectedly, we have found

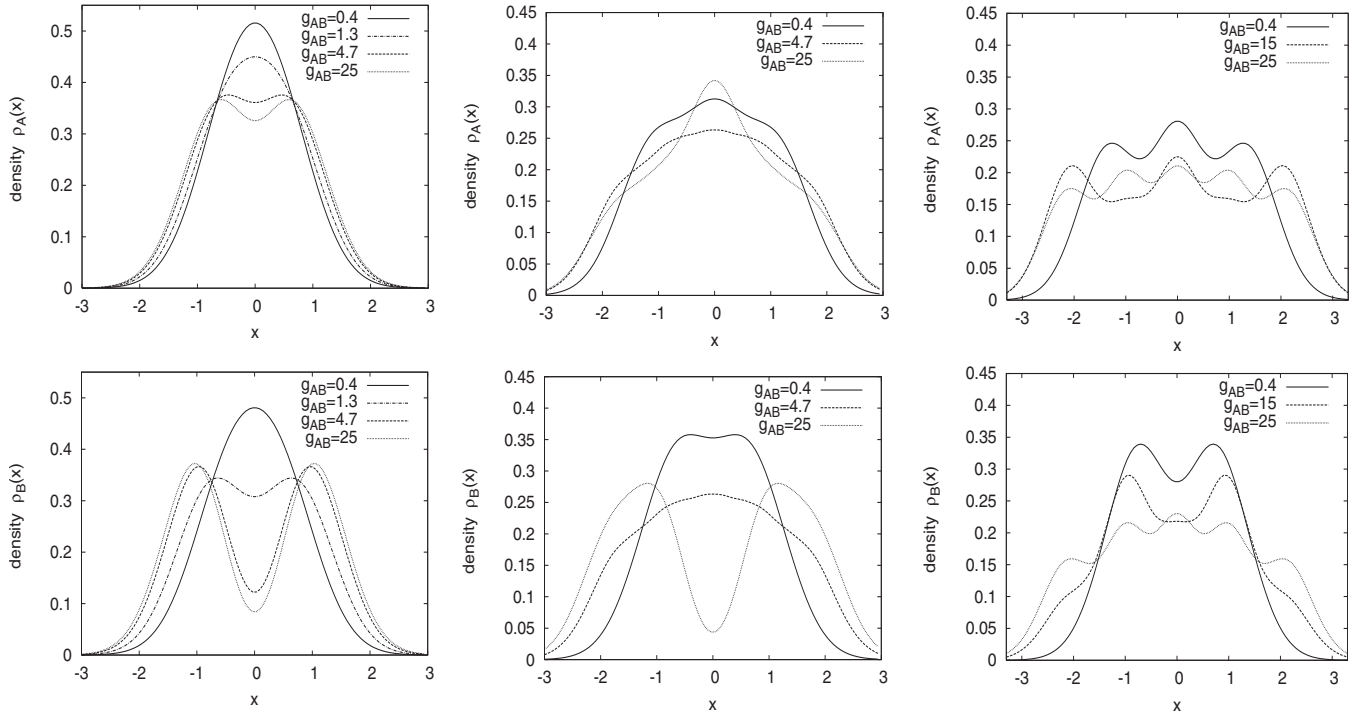


FIG. 5. Demixing for different particle numbers $N_A=3$, $N_B=2$: Density profiles $\rho_A(x)$ (top) and $\rho_B(x)$ (bottom) for intraspecies interaction strengths $g_\sigma=0.4$, 4.7, and 25 (from left to right).

this to be even more pronounced for $N_A \gg N_B$. Note that, close to the composite-fermionization limit ($g_{AB}=4.7, 25$), both components develop two humps in the density, if much more pronounced for B . This is indicative of a superposition state similar to that in Sec. IV: The B atoms are found on the right and the A atoms on the left, and vice versa, only that the shift for A atoms is much smaller due to their higher density.

A similar pathway again exists for non-negligible intra-component interactions, $g_\sigma=4.7$ (Fig. 5). As $g_{AB} \rightarrow \infty$, the initially mixed phases separate: The profile $\rho_A(x)$ develops a clear-cut peak at $x=0$, whereas B is again driven to the boundary. Even though, on the face of it, this looks different from the weakly interacting case, this density pattern can be understood in complete analogy: The two components are isolated on the left and on the right, respectively; however, due to the larger atom number N_A and the repulsion pressure, A tends to be more in the center *on average*.

An entirely different situation is encountered in the ‘‘Fermi-Fermi’’-type setup with $g_\sigma=25$ (Fig. 5). For intermediate $g_{AB}=15 < g_\sigma$, a phase forms where the A atoms localize at three discrete spots such that the two B atoms completely localize atom by atom just like in the case of a 2+2 mixture, in agreement with the extended Bose-Fermi map (1). In analogy to Sec. IV, these will demix under slight symmetry-breaking perturbations into one phase with $N_A=3$ density wiggles on, say, the left side, and $N_B=2$ on the right.

B. Interaction-assisted demixing

Up until now, we have assumed comparable interactions within each component. Of course, it is of fundamental con-

cern what the composite-fermionization crossover looks like in the case where one species is more strongly repulsive, including as a special case a ‘‘Bose-Fermi’’-type mixture of one weakly interacting and another fermionized component. An illustrative example is given in Fig. 6, displaying the composite-fermionization crossover for an $N_\sigma=2$ mixture with $g_A=4.7 > g_B=0.4$. We distinguish two regimes.

(1) For $g_{AB} < g_A$, the weakly interacting central B cloud is barely affected; at the same time, the strongly interacting A bosons move slightly to the outside, thus cutting down on both intra- and interspecies interaction energy.

(2) By contrast, for $g_{AB}=25 > g_A$, this partial separation is no longer enough: Now the B cloud splits up, signifying the formation of the entangled state discussed before with N_A atoms on the left and N_B atoms on the right, and vice versa. Note that, owing to the strong intraspecies repulsion in A , the two humps in ρ_A are washed out strongly.

We stress that only regime 1 exists for a Bose-Fermi-type mixture, i.e., where $g_A \rightarrow \infty$: The minimum-energy state for infinitely large g_{AB} then has all B atoms in the center and A on the edges.

Coherence aspects

At this point, it is worthwhile dwelling for a moment on the coherence properties of bosonic mixtures, as reflected in the reduced one-body density matrix $\rho_\sigma(x, x') \equiv \langle x | \hat{\rho}_\sigma^{(1)} | x' \rangle$ and, closely related, the momentum distribution

$$\tilde{\rho}_\sigma(k) \equiv 2\pi \langle k | \hat{\rho}_\sigma^{(1)} | k \rangle = \int dx \int dx' e^{-ik(x-x')} \rho_\sigma(x, x').$$

It has been demonstrated for *identical* bosons [29,30] how, in

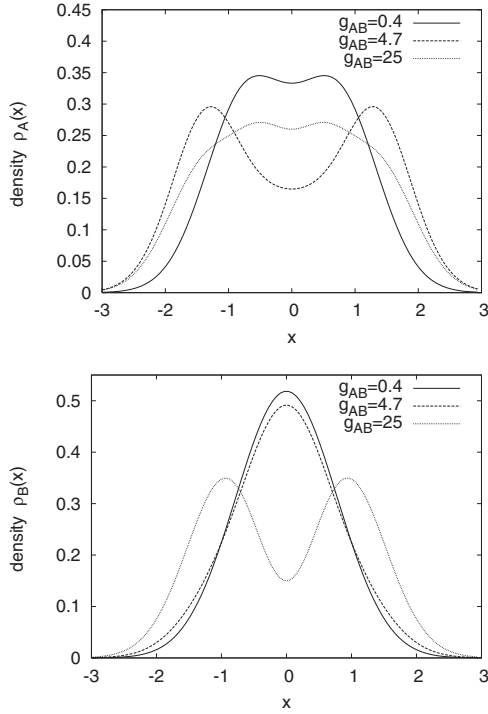


FIG. 6. Demixing for different intracomponent interactions $g_A = 4.7$, $g_B = 0.4$: Density profiles $\rho_A(x)$ (top) and $\rho_B(x)$ (bottom) for an $N_\sigma = 2$ mixture at different couplings $g_{AB} = 0.4, 4.7$, and 25 .

the course of fermionization, the zero-momentum peak $\tilde{\rho}(k=0)$ —related to the fraction of condensed bosons—is attenuated and redistributed toward higher momenta, culminating in a characteristic decay $\tilde{\rho}(k) \xrightarrow{k \rightarrow \infty} ck^{-4}$ as predicted for hard-core short-range interactions [42]. Equivalently, the off-diagonal long-range order, measured by $\rho_1(x, -x)$ as $x \rightarrow \infty$, is strongly reduced. We generally find the same two mechanisms at work here, which we exemplify in Fig. 7. For stronger interspecies repulsion, the high-momentum tail in $\tilde{\rho}_\sigma(k)$ becomes more pronounced. Interestingly, for the component B with weaker interaction, the $k=0$ peak starts diminishing right away, while the strongly repulsive A component first sees a sharpening at zero momentum ($g_{AB} = 4.7$). This derives from its initial delocalization so as to move away from B [cf. $\rho_A(x_A, x'_A)$ in Fig. 7], which allows the A atoms to spend less kinetic energy $\langle \frac{1}{2}p^2 \rangle \propto (\Delta k)^2$.

C. Trap-induced demixing

After having explored the effect of different densities or interaction strengths on the composite-fermionization pathway, let us now relax the condition of equal masses and trapping potentials (here, frequencies). In this case, the system no longer maps to a single-component Bose gas even for $g_\sigma = g_{AB}$.

1. Different confinement lengths

Assume that we have a nontrivial mass ratio, i.e., $M_B > 1$, without loss of generality, with an otherwise symmetric parameter set. The effective oscillator length of the B atoms

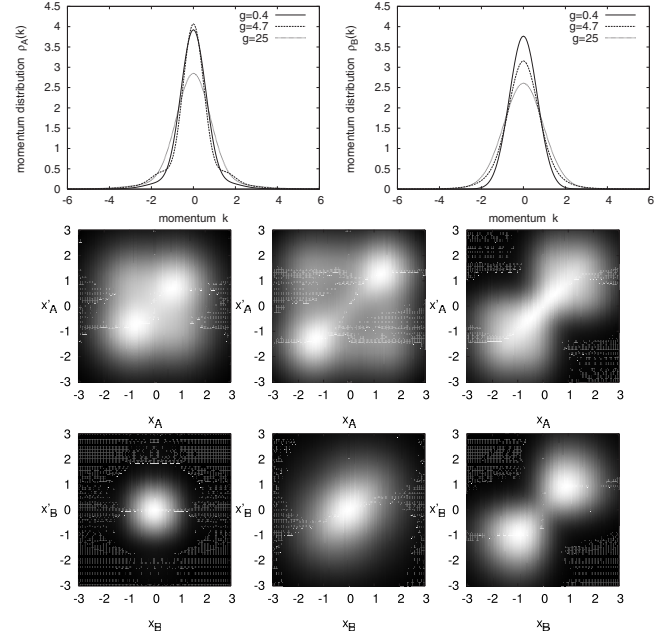


FIG. 7. Coherence properties of the system in Fig. 6. Top: momentum distributions $\tilde{\rho}_\sigma(k)$; bottom: one-body density matrices $\rho_\sigma(x_\sigma, x'_\sigma)$ for $g_{AB} = 0.4, 4.7$, and 25 (from left to right).

will then be reduced by a factor of $a_B = 1/\sqrt{M_B} < 1$. This situation is visualized in Fig. 8 for the choice $M_B = 9$. At weak couplings, $\rho_B(x)$ is simply constricted at the trap center, while $\rho_A(x)$ extends over a much larger region. As we switch on the interaction between the components, the B atoms remain unmoved, whereas the A bosons are gradually driven

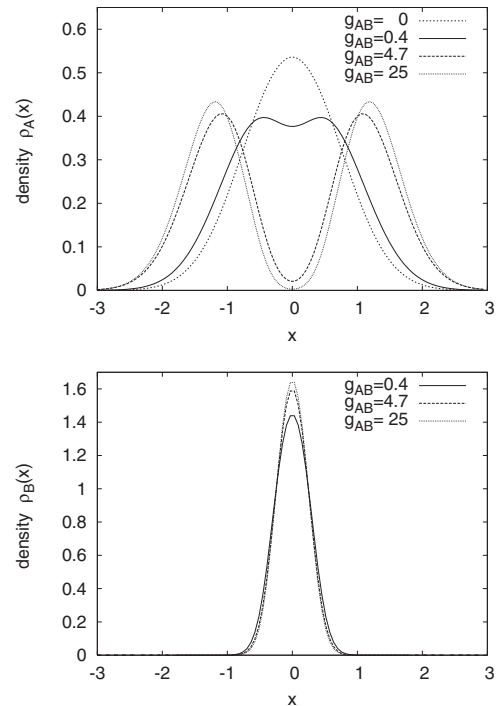


FIG. 8. Demixing for different masses $M_B/M_A = 9$: Density profiles $\rho_A(x)$ (top) and $\rho_B(x)$ (bottom) for a $2+2$ mixture with $g_\sigma = 0.4$ at different couplings g_{AB} .

toward the outside. This is intuitive: The former component roughly experiences an average Hamiltonian

$$\bar{H}_B = H_B + \text{tr}_A(H_{AB}\hat{\rho}_A^{(N_A)}) = H_B + g_{AB}N_A \sum_{b=1}^{N_B} \rho_A(x_{B,b}),$$

and likewise for A . Since the heavy B atoms are effectively frozen at the center, where $\rho_A(x_B) \approx \rho_A(0)$ changes slowly, they experience only a constant energy shift due to the presence of A atoms. By contrast, the latter see an effective “potential barrier” $\rho_B(x_A) \approx \delta(x_A)$ which varies only in a small region about zero.

That phase-separation mechanism is largely insensitive to the intraspecies interactions g_σ : We have confirmed these results also for, e.g., two nearly fermionized components. Also note that a similar scale separation persists for the case of different frequencies but equal masses, i.e., $\omega_B/\omega_A \gg 1$. The different effective interaction experienced by B , $g'_B = g_B\sqrt{M_B/\omega_B}$, and the modified energy scale ω_B do not qualitatively alter the picture above.

2. Different energy scales

Let us now look into the complementary case where the oscillator lengths are equal, $a_B = 1/\sqrt{M_B\omega_B} = 1$, but such that the energy scale $\omega_B \neq 1$ is different. In other words, a stronger localization by virtue of a larger mass is compensated by a shallower trap for the B species. This option is investigated in Fig. 9, where $M_B = 3 = \omega_B^{-1}$. The two profiles still overlap for weak couplings $g_{AB} = 0, 1.3$. For sufficiently strong interspecies repulsion, though, it apparently becomes beneficial for the B atoms to spread out to larger x so as to segregate from A , which in turn is compressed on the inside. This is particularly striking in the setup captured in Fig. 9: Here the A component is squeezed even though it is fermionized and thus possesses a high internal pressure. The reason for that counterintuitive behavior is simply that the potential-energy costs for the B phase are lower by $\omega_B = 1/3$.

VI. CONCLUSION

We have studied binary few-boson mixtures in a one-dimensional harmonic trap throughout the crossover from weak coupling to strong intercomponent repulsion. Depending on the intraspecies interactions, different pathways to composite fermionization have shown up: For two weakly interacting Bose gases, the two phases segregate as a whole, where the demixing for equal densities is obscured by symmetry-induced entanglement fragile to displacement of the trap. By contrast, for two strongly repulsive components, the atoms localize one by one.

If one component has a lower density, then it tends to delocalize toward the outer edge, while the high-density phase is compressed in the center. Furthermore, when one component is far more repulsive, the crossover exhibits an

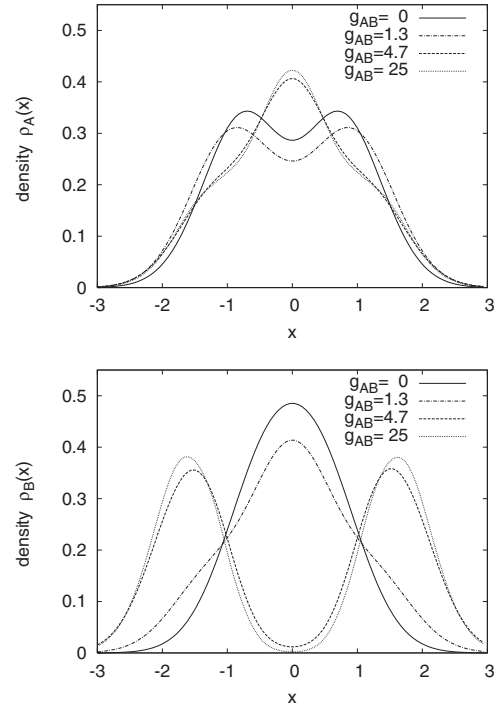


FIG. 9. Demixing for different energy scales $M_B = 1/\omega_B = 3$: Density profiles $\rho_A(x)$ (top) and $\rho_B(x)$ (bottom) for a 2+2 mixture with $g_A = 25$ and $g_B = 0.4$, at different couplings g_{AB} .

intermediate regime where that species forms a shell around the central, weakly interacting, component; only for large interspecies couplings do they fully segregate. This is accompanied by an increase (decrease) of the central momentum peak for the strongly (weakly) interacting species. Finally, for different mass or frequency ratios, one component freezes at the trap center, such that it acts as an effective potential barrier for the more mobile species.

The small mixtures of strongly repulsive atoms studied here should be experimentally accessible. The preparation and detection techniques required are similar to those already available for few bosons of a single species. The interaction forces may be tuned independently over a wide range by varying the (inter- and intraspecies) scattering lengths as well as the transverse confinement, which parametrically modifies the effective one-dimensional coupling strengths.

Note added: Recently we have become aware of related work by Hao *et al.* [43].

ACKNOWLEDGMENTS

Financial support from the Landesstiftung Baden-Württemberg in the framework of the project “Mesoscopics and Atom Optics of Small Ensembles of Ultracold Atoms” is acknowledged by P.S. and S.Z. We also thank F. Deuretzbacher for fruitful discussions (S.Z.).

- [1] C. J. Pethick and H. Smith, *Bose-Einstein Condensation in Dilute Gases* (Cambridge University Press, Cambridge, U.K., 2001).
- [2] L. Pitaevskii and S. Stringari, *Bose-Einstein Condensation* (Oxford University Press, Oxford, 2003).
- [3] A. G. Truscott *et al.*, *Science* **291**, 2570 (2001).
- [4] Z. Hadzibabic, C. A. Stan, K. Dieckmann, S. Gupta, M. W. Zwierlein, A. Gorlitz, and W. Ketterle, *Phys. Rev. Lett.* **88**, 160401 (2002).
- [5] M. Taglieber, A. C. Voigt, T. Aoki, T. W. Hansch, and K. Dieckmann, *Phys. Rev. Lett.* **100**, 010401 (2008).
- [6] C. J. Myatt, E. A. Burt, R. W. Ghrist, E. A. Cornell, and C. E. Wieman, *Phys. Rev. Lett.* **78**, 586 (1997).
- [7] D. S. Hall, M. R. Matthews, J. R. Ensher, C. E. Wieman, and E. A. Cornell, *Phys. Rev. Lett.* **81**, 1539 (1998).
- [8] P. Maddaloni, M. Modugno, C. Fort, F. Minardi, and M. Inguscio, *Phys. Rev. Lett.* **85**, 2413 (2000).
- [9] G. Modugno, M. Modugno, F. Riboli, G. Roati, and M. Inguscio, *Phys. Rev. Lett.* **89**, 190404 (2002).
- [10] J. Catani, L. DeSarlo, G. Barontini, F. Minardi, and M. Inguscio, *Phys. Rev. A* **77**, 011603(R) (2008).
- [11] M. A. Cazalilla and A. F. Ho, *Phys. Rev. Lett.* **91**, 150403 (2003).
- [12] Y.-Q. Li, S.-J. Gu, Z.-J. Ying, and U. Eckern, *Europhys. Lett.* **61**, 368 (2003).
- [13] V. S. Shchesnovich, A. M. Kamchatnov, and R. A. Kraenkel, *Phys. Rev. A* **69**, 033601 (2004).
- [14] O. E. Alon, A. I. Streltsov, and L. S. Cederbaum, *Phys. Rev. Lett.* **97**, 230403 (2006).
- [15] T. Mishra, R. V. Pai, and B. P. Das, *Phys. Rev. A* **76**, 013604 (2007).
- [16] T. Roscilde and J. I. Cirac, *Phys. Rev. Lett.* **98**, 190402 (2007).
- [17] K. Nho and D. P. Landau, *Phys. Rev. A* **76**, 053610 (2007).
- [18] A. Kleine, C. Kollath, I. P. McCulloch, T. Giamarchi, and U. Schollwöck, *Phys. Rev. A* **77**, 013607 (2008).
- [19] T. Köhler, K. Góral, and P. S. Julienne, *Rev. Mod. Phys.* **78**, 1311 (2006).
- [20] M. Olshanii, *Phys. Rev. Lett.* **81**, 938 (1998).
- [21] T. Kinoshita, T. Wenger, and D. S. Weiss, *Science* **305**, 1125 (2004).
- [22] B. Paredes *et al.*, *Nature (London)* **429**, 277 (2004).
- [23] M. Girardeau, *J. Math. Phys.* **1**, 516 (1960).
- [24] D. S. Petrov, G. V. Shlyapnikov, and J. T. M. Walraven, *Phys. Rev. Lett.* **85**, 3745 (2000).
- [25] V. Dunjko, V. Lorent, and M. Olshanii, *Phys. Rev. Lett.* **86**, 5413 (2001).
- [26] O. E. Alon and L. S. Cederbaum, *Phys. Rev. Lett.* **95**, 140402 (2005).
- [27] Y. Hao, Y. Zhang, J. Q. Liang, and S. Chen, *Phys. Rev. A* **73**, 063617 (2006).
- [28] S. Zöllner, H.-D. Meyer, and P. Schmelcher, *Phys. Rev. A* **74**, 053612 (2006).
- [29] S. Zöllner, H.-D. Meyer, and P. Schmelcher, *Phys. Rev. A* **74**, 063611 (2006).
- [30] F. Deuretzbacher, K. Bongs, K. Sengstock, and D. Pfannkuche, *Phys. Rev. A* **75**, 013614 (2007).
- [31] M. D. Girardeau and A. Minguzzi, *Phys. Rev. Lett.* **99**, 230402 (2007).
- [32] H.-D. Meyer, U. Manthe, and L. S. Cederbaum, *Chem. Phys. Lett.* **165**, 73 (1990).
- [33] M. H. Beck, A. Jäckle, G. A. Worth, and H.-D. Meyer, *Phys. Rep.* **324**, 1 (2000).
- [34] S. Zöllner, H.-D. Meyer, and P. Schmelcher, *Phys. Rev. A* **75**, 043608 (2007).
- [35] S. Zöllner, H.-D. Meyer, and P. Schmelcher, *Phys. Rev. Lett.* **100**, 040401 (2008).
- [36] S. Zöllner, H.-D. Meyer, and P. Schmelcher, *Phys. Rev. A* **78**, 013621 (2008).
- [37] R. Kosloff and H. Tal-Ezer, *Chem. Phys. Lett.* **127**, 223 (1986).
- [38] H.-D. Meyer and G. A. Worth, *Theor. Chem. Acc.* **109**, 251 (2003).
- [39] M. A. Cirone, K. Góral, K. Rzazewski, and M. Wilkens, *J. Phys. B* **34**, 4571 (2001).
- [40] M. D. Girardeau, E. M. Wright, and J. M. Triscari, *Phys. Rev. A* **63**, 033601 (2001).
- [41] E. B. Kolomeisky, T. J. Newman, J. P. Straley, and X. Qi, *Phys. Rev. Lett.* **85**, 1146 (2000).
- [42] A. Minguzzi, P. Vignolo, and M. P. Tosi, *Phys. Lett. A* **294**, 222 (2002).
- [43] Y. Hao and S. Chen, e-print arXiv:0804.1991.